Published in final edited form as:
Magn Reson Med. 2012 September ; 68(3): 680–689. doi:10.1002/mrm.23267.

Comparison of Optimized Soft-Tissue Suppression Schemes for Ultra-short Echo Time (UTE) MRI

Cheng Li, **Jeremy F. Magland**, **Hamidreza Saligheh Rad**, **Hee Kwon Song**, and **Felix W. Wehrli**
Department of Radiology, University of Pennsylvania, Philadelphia, PA 19104, USA

Abstract

Ultra-short echo time (UTE) imaging with soft-tissue suppression reveals short-T_2 components (typically hundreds of microseconds to milliseconds) ordinarily not captured or obscured by long-T_2 tissue signals on the order of tens of milliseconds or longer. The technique therefore enables visualization and quantification of short-T_2 proton signals such as those in highly collagenated connective tissues. This work compares the performance of the three most commonly used long-T_2 suppression UTE sequences, i.e. echo subtraction (dual-echo UTE), saturation via dual-band saturation pulses (dual-band UTE), and inversion by adiabatic inversion pulses (IR-UTE) at 3T, via Bloch simulations and experimentally *in vivo* in the lower extremities of test subjects. For unbiased performance comparison, the acquisition parameters are optimized individually for each sequence to maximize short-T_2 SNR and CNR between short- and long-T_2 components. Results show excellent short-T_2 contrast is achieved with these optimized sequences. A combination of dual-band UTE with dual-echo UTE provides good short-T_2 SNR and CNR with less sensitivity to B_1 homogeneity. IR-UTE has the lowest short-T_2 SNR efficiency but provides highly uniform short-T_2 contrast and is well suited for imaging short-T_2 species with relatively short T_1 such as bone water.

Keywords

Ultra-short Echo Time (UTE) Imaging; Long-T_2 Suppression; Short-T_2 Contrast; Imaging Parameter Optimization

Introduction

During the past decade, ultra-short echo time (UTE) MRI has evolved into a promising technique for imaging tissue components with very short T_2 relaxation time of hundreds of microseconds to a few milliseconds (1-5). The collagenated structures of the musculoskeletal system, such as cortical bone, cartilage, tendons, and other connective tissues, are the exemplary short-T_2 species and subject to restricted mobility of water either bound to collagen or confined to small spaces (6). Other examples include lung tissue (7), myelin (8), calcifications (9,10) and ^{31}P in bone mineral (11). These components typically show very low or no signal in conventional MRI obtained with echo times (TE) of several milliseconds or longer. In conjunction with specifically designed RF pulses and sampling strategy, UTE imaging has been shown to achieve effective TEs of 100 μs or less depending on the MR system hardware, thereby capturing a significant portion of the signal arising from short-T_2 nuclei.

Corresponding Author: Felix W. Wehrli, Ph.D. Laboratory for Structural NMR Imaging Department of Radiology, University of Pennsylvania 1 Founders Pavilion, 3400 Spruce Street Philadelphia, PA 19104.

Although short-T_2 species become detectable in UTE imaging, their signals are often obscured by the much more intense signals of the surrounding long-T_2 components, which usually have far higher proton density. To better visualize the short-T_2 protons, long-T_2 suppression techniques are commonly employed in UTE imaging (1). Generally, the goal of long-T_2 suppression is to maximize suppression of the long-T_2 components while preserving the short-T_2 components. Several methods have been proposed for soft-tissue suppression and short-T_2 species contrast enhancement which can be categorized into two types: a combination of different TEs, or some form of magnetization preparation involving either saturation or inversion nulling.

The first type is perhaps the most common and simplest, in which an image obtained with longer TE, containing signal principally from long-T_2 protons only, is subtracted from a short-TE image (1). The main benefit of this approach is that it is simple and can easily be incorporated into 2D and 3D UTE sequences without significant sequence modification or increase in scan time. However, T_2* losses and SNR reduction from the subtraction operation may degrade the quality of soft-tissue suppression. The first of the magnetization preparation based soft-tissue suppression techniques was proposed by Pauly et al. (12), i.e. T_2-Selective RF Excitation Contrast or TELEX, in which a long rectangular $\pi/2$ saturation pulse is applied followed by a spoiler gradient preceding short RF pulse excitation. The long saturation pulse selectively excites the long-T_2 species while leaving the short-T_2 components largely unperturbed since their decay rate exceeds the excitation rate. An improved version of this technique, referred to as refocused TELEX (13), reduces the sensitivity of the original method to B_0 inhomogeneity by interrupting the long $\pi/2$ pulse using a series of short refocusing pulses to broaden the bandwidth of the saturation pulse. However, the performance of this approach varies with T_1/T_2.

Recently, several research groups reported various improved long-T_2 suppression methods (14-18), based either on saturation or inversion pulses. Larson et al. designed single-band and dual-band maximum-phase saturation pulses (15) using the Shinnar-Le Roux (SLR) design tools with complex Parks-McClellan algorithm (19). The beneficial feature of SLR design algorithm is that the designer has the freedom to specify the pulse parameters, such as pulse duration, suppression bandwidth and desired ripple values for each band. These saturation pulses created good short-T_2 contrast at 1.5 T. However, they are sensitive to B_1 inhomogeneity, causing nonuniform soft-tissue suppression. To overcome the sensitivity to B_1 field variation, long adiabatic inversion pulses can be employed to invert the long-T_2 components, while affecting to a lesser extent the short-T_2 species, then followed by UTE acquisition at the null point of the long-T_2 components (1). Recently, two variants of this approach have appeared. Larson et al. used phase-sensitive inversion recovery at 1.5 T to allow UTE acquisition immediately after the adiabatic inversion pulse by combining the images with inversion preparation with those collected without preparation pulses (16). Du et al. proposed dual inversion-recovery UTE (DIR-UTE) (17) in which two long adiabatic inversion pulses centered on the water and fat resonance frequencies are applied to account for the T_1 difference between water and fat.

Other magnetization-preparation based soft-tissue suppression methods exist as well. In work performed on a 4.7 T small-bore system Wu et al. used two long rectangular $\pi/2$ pulses placed on resonance with fat and water, executed with and without π pulses in two successive scans added to cancel the effect of $\pi/2$ pulse imperfections in what they termed water- and fat-suppressed proton projection MRI (WASPI) (14,20). However, because of the greater B_1 variation on a clinical scanner and doubled imaging time due to the need for two scans, only two long rectangular $\pi/2$ pulses were applied in this more recent implementation of the WASPI technique (21). Thus, the long-T_2 suppression portion of this embodiment of WASPI is essentially identical to TELEX. Du et al. conceived the technique called UTE

with off-resonance saturation contrast (UTE-OSC) (18), in which two images with and without application of a high-power off-resonance saturation pulse are acquired. Short-T_2 contrast is achieved by subtraction of the two images. One possible problem with this approach is that the subtraction operation and magnetization transfer effect may impair the effectiveness of long-T_2 suppression.

Given the many long-T_2 suppression schemes available, comparison of their performance would provide insight and guide their use in research and clinical applications. Although several research groups compared some soft-tissue suppression approaches (22,23), these comparisons were not based on optimal imaging protocols and the results therefore were not conclusive.

In this work, we compared the performance of the three most commonly used soft-tissue suppression schemes, echo subtraction using two different TEs (termed as dual-echo UTE), saturation via dual-band saturation pulses (dual-band UTE) and inversion by adiabatic inversion pulses (IR-UTE) at 3 T, via Bloch equation simulations and experimentally *in vivo* in the lower extremities of test subjects. The strategy adopted that allows for unbiased performance comparison entails optimization of the acquisition parameters individually for each method to maximize short-T_2 SNR and CNR between short- and long-T_2 components. Based on the outcome of these experiments for the target short-T_2 tissues (bone and tendon), the performance of the various methods examined was quantitatively evaluated.

Theory

For unbiased comparison of the various soft-tissue suppression methods, the acquisition parameters for each of the three pulse sequences need to be optimized to maximize SNR of short-T_2 species and CNR between short- and long-T_2 components. We define SNR efficiency (SNR_{eff}) as image SNR normalized by the square-root of total scan time for the purpose of comparing sequences with different imaging times. Image SNR depends on field strength, T_1, T_2, voxel dimensions, pulse sequence type and timing parameters, and total sampling time. Since the long-T_2 suppression methods are variants of the original UTE sequence, the imaging parameters to be optimized reduce to a small set, including TR, flip angle of the half excitation pulse and magnetization preparation pulses, with all other parameters being held constant. In the following we describe each pulse sequence and the relevant parameters for optimizing long-T_2 suppression and short-T_2 SNR_{eff}.

Dual-echo UTE

Dual-echo UTE is the most commonly used method for soft-tissue suppression. As shown in the pulse sequence diagram (Fig.1), two identical half radial projections differing in echo times are acquired after each half-pulse excitation. The long-TE image, containing signal predominantly from long-T_2 species, is subtracted from the first echo image, which contains both long and short-T_2 species. The resulting difference creates an image highlighting the short-T_2 tissue components. Assuming that the magnetization reaches the steady state and there is negligible short-T_2 proton signal in the second TE image, SNR_{eff} of short-T_2 species in dual-echo UTE can be written as:

$$SNR_{eff} \propto f_{xy} \frac{1 - \exp(-TR/T_1)}{\sqrt{2}\,(1 - f_z \exp(-TR/T_1))\,\sqrt{T_{acq}}} \quad [1]$$

where f_{xy}, f_z representing the normalized transverse and longitudinal magnetizations in response to the excitation pulse (13) deviate from the usual sine and cosine terms of the flip angle due to the evolution of the magnetization during the finite duration of the pulse relative to T_2, and need to be numerically evaluated from the Bloch equations. T_{acq} is the

total sampling time, which is proportional to TR. The factor $\sqrt{2}$ results from the subtraction operation.

Dual-band UTE

Dual-band UTE involves magnetization-preparation based soft-tissue suppression, in which a long dual-band saturation pulse is played out before the UTE acquisition in order to suppress the long-T_2 species. The dual-band pulse has two spectral saturation bands at water and fat resonances, which can be designed using SLR algorithm with complex Parks-McClellan algorithm (15,19). Since lipid protons have multiple resonance peaks and relaxation times considerably shorter than those of water protons, the optimal flip angle of the saturation pulse for fat may be different from water. Therefore, we included the flip angles for both water and fat as design variables, along with the pulse duration, filter order, fat resonance frequency, desired ripple values and suppression bandwidth corresponding to the range of the off-resonance frequencies. Considering the effect of dual-band pulse on short-T_2 species, SNR_{eff} can be expressed as follows, assuming magnetization is in the steady state:

$$SNR_{eff} \propto f_{xy}\frac{f_{z,dualband}\left(1-\exp\left(-\left(TR-T_{dualband}\right)/T_1\right)\right)}{\left(1-f_{z,dualband}f_z\exp\left(-\left(TR-T_{dualband}\right)/T_1\right)\right)\sqrt{T_{acq}}} \quad [2]$$

where $f_{z,dualband}$ is the normalized longitudinal magnetization in response to the dual-band pulse. This can be calculated by numerical solution of the Bloch Equations. Quantities f_{xy}, f_z and T_{acq} have previously been defined, and $T_{dualband}$ is the dual-band pulse duration. From Eq.2, we can see that the SNR of short-T_2 species depends on the dual-band saturation pulse, the excitation pulse and TR. Since the dual-band pulse has already been designed to maximally suppress the long-T_2 components, its saturation effect on short-T_2 species could be predetermined by the Bloch equation evaluation prior to optimizing the excitation pulse and TR.

IR-UTE

IR-UTE is a soft-tissue suppression method in which a long adiabatic pulse inverts the long-T_2 components while only slightly perturbing the short-T_2 protons, followed by UTE acquisition at the null point of the long-T_2 components. This method is relatively immune to spatial B_1 variations because of the properties of adiabatic pulses. A potential difficulty with IR-UTE is achieving simultaneous nulling of both types of protons given the significantly different T_1 relaxation times of water and fat protons. However, it turns out that for TR < T_1 optimal inversion delays for water and fat are close (i.e. differing by a few milliseconds), thereby resulting in negligible residual longitudinal magnetization at the time-point of sampling the UTE signal. Including the effect of the adiabatic inversion pulse and assuming the magnetization to have reached a steady state, SNR_{eff} for the short-T_2 protons is calculated according to:

$$SNR_{eff} \propto f_{xy}\frac{1-\left(1-f_{z,inv}\right)\exp\left(-TI/T_1\right)-f_{z,inv}\exp\left(-\left(TR-T_{inv}\right)/T_1\right)}{\left(1-f_{z,inv}f_z\exp\left(-\left(TR-T_{inv}\right)/T_1\right)\right)\sqrt{T_{acq}}} \quad [3]$$

In Eq. 3 $f_{z,inv}$ is the normalized longitudinal magnetization of the short-T_2 protons in response to the adiabatic inversion pulse. T_{inv} is the adiabatic inversion pulse duration. TI is the inversion time, defined as the time interval between the end of the adiabatic pulse and the start of the half-sinc pulse. Short-T_2 SNR is a function of the inversion pulse, TI, excitation pulse and TR. The inversion pulse, TR and TI are optimized to suppress the long-T_2 species. The effect of the adiabatic inversion pulse on short-T_2 components was

evaluated by numerically solving the Bloch equations, and the optimal flip angle of the excitation pulse was determined from Eq.3.

Methods and Materials

For each of the three sequences, the adjustable parameters described above were first optimized to maximize soft-tissue suppression, including TE_2 (dual-echo UTE), dual-band pulse (dual-band UTE), and adiabatic inversion pulse, TR and TI (IR-UTE), The imaging parameters were then chosen to maximize short-T_2 SNR_{eff}. After initially optimizing the imaging parameters for each sequence via Bloch equation simulations, the optimized sequences were used to acquire *in vivo* images for cortical bone and Achilles tendon, and SNR and CNR of the three sequences were compared to evaluate their performance.

Tissue Parameters

To optimize the imaging parameters for each sequence, the relaxation times for the target tissue components needed to be determined first as input parameters for the Bloch equation simulations and computation of SNR. Although there is significant age dependence of relaxation times in cortical bone and Achilles tendon (for example, in cortical bone as a result of porosity and pore size (24)), the typical T_1 and T_2 relaxation times used in the optimization procedures were: $T_{1,bone}$ = 200 ms, $T_{2,bone}$ = 420 μs (25), $T_{1,tendon}$ = 600 ms, $T_{2,tendon}$ = 1 ms (26,27).

Imaging Parameter Optimizations

The critical variable determining the effectiveness of soft-tissue suppression in dual-echo UTE is the second TE, which needs to be chosen to allow adequate short-T_2 signal decay while minimally affecting the long-T_2 components. To avoid signal cancellation from long-T_2 components with different chemical shifts, the water and fat methylene resonances should be in phase at TE_2, i.e., at an integer multiple of 2.3 ms at 3 T. The durations for sampling of the first echo and readout rewinding gradients limit TE_2 to a minimum of 4.6 ms.

For dual-band UTE, the dual-band pulse must be optimized to achieve maximal soft-tissue suppression. As stated in the theory section, the optimal flip angle of the saturation pulse for fat may differ from that for water. To determine optimal saturation pulse flip angles, we first designed a series of conventional dual-band pulses with flip angles from 80° to 130° degrees in steps of 5°. These preparation pulses were then incorporated into a spoiled gradient echo sequence to image a phantom consisting of containers of distilled water doped with 0.09 mM $MnCl_2$ and 0.2M NaCl and vegetable oil with the following parameters: FOV = 200×200 mm^2, slice thickness of 5 mm, matrix size = 256×256, TR = 200 ms, TE = 4 ms. SNR of both water and fat images were calculated and plotted as a function of the flip angle of the dual-band saturation pulse. As suggested in Fig. 2, the optimal flip angle to produce minimal water signal is 100°, while for fat it is 110°. Once the optimal flip angles for water and fat were obtained, a dual-band pulse with different flip angles on water and fat bands was designed using the SLR and complex Parks-McClellan algorithms. The design function was derived from Larson et al's dual-band pulse design function (15), which includes flip angles for water and fat, pulse duration, filter order, fat resonance frequency, desired ripple values and suppression bandwidths as input design parameters. We chose a pulse duration of 15 ms, filter order of 300, flip angles of 100° for water and 110° for fat, suppression bandwidths of 120 Hz on resonance and 320 Hz at the fat resonance centered at -430 Hz at 3T, and ripple values of 0.5% for all the *in vivo* experiments. To validate the performance of the dual-band pulse, its off-resonance and T_2 profiles were evaluated using matrix-form

Bloch equation simulation (28). For off-resonance simulation, T_2 = 100 ms, T_1 = 1 s were used with frequencies between -800 Hz and 400 Hz relative to water protons.

The adiabatic inversion pulse, TR and TI are the parameters to be optimized to suppress the long-T_2 species in IR-UTE. A hyperbolic secant (HS) adiabatic inversion pulse was used in all *in vivo* experiments. To minimize bone water suppression and maximally suppress the long-T_2 components, the HS pulse was optimized as follows: 1) Pulse bandwidth/duration = 1 kHz/20 ms, with a frequency shift of 270 Hz towards the lipid peak in order to cover both fat and water peaks; 2) The frequency was swept from higher to lower frequency, inverting water before fat to compensate for the longer T_1 of water; 3) The HS pulse amplitude was set to allow 30% B_1 variation. Bloch equation simulations were performed to evaluate the off-resonance and T_2 profiles of the HS pulse and overall performance. T_2 = 100 ms, T_1 = 1 s were used in the off-resonance simulation. Water and fat longitudinal magnetizations could not be completely nulled simultaneously because of their very different T_1 values. However, as pointed out previously, their null time points (i.e. TIs), are relatively close when TR is short and the magnetization has reached a steady state. Based on Ref. (29) and of some of the authors' previous work (30), a combination of TR = 300 ms and TI = 100 ms is a good balance between short-T_2 SNR and long-T_2 suppression..

After the soft-tissue suppression related parameters were determined, other imaging parameters were optimized to maximize the SNR_{eff} of the target short-T_2 species for each sequence according to Eqs. 1-3. The effects of dual-band pulse, HS pulse and half excitation pulse were calculated by Bloch equation simulation. The parameters of the dual-band and HS pulses have been described above. The parameters for the Hamming filtered half-sinc variable rate-selective excitation (VERSE) pulse (31) were as follows: pulse duration = 830 μs with 580 μs played out at the plateau and 250 μs at the ramp-down of the slice selection gradient (bandwidth = 4258 Hz creating 5mm slice thickness with 20 mT/m slice selection gradient). For dual-echo UTE and dual-band UTE, TR and flip angle of the half excitation pulse were optimized, while in IR-UTE, only the optimal flip angle of the half excitation pulse needs to be determined. In the case where the optimal excitation flip angle was close to 90°, the half-sinc pulse was replaced by a half-SLR pulse (32) in the subsequent *in vivo* scans as a means to improve the slice profile. All pulse design tasks, simulations and optimizations were implemented with MATLAB (Mathworks, Natick, MA, USA) using in-house programs.

Human Subject Studies

All *in vivo* MRI scans were performed at 3T (TIM Trio; Siemens Medical Solutions, Erlangen, Germany). The mid-tibia (38% site as measured from the lateral malleolus) and Achilles tendon of five healthy volunteers (age range: 24-40 years; gender: 3 males and 2 females) were imaged with all the three sequences. The protocol for this study was approved by the Institutional Review Board and informed written consent was obtained for each participant. The same scan parameters were used for the UTE acquisition portion of the three sequences to ensure unbiased comparison (slice thickness = 5 mm, TE_1/TE_2 = 60 μs/ 4.6 ms). For the dual-TE sequence 2000 ramp-sampled half-radial projections were acquired (corresponding to 24% oversampling) to achieve adequate SNR considering the short TR (20 ms). For the other two sequences (dual-band and IR-UTE) only 500 projections were acquired (corresponding to an undersampling factor of 3.2) in order to reduce total scan time, given the much longer TR required by these sequences (see Table 1). We note here that the superior long-T_2 suppression tolerates some undersampling without causing apparent streaking artifacts. In order to drive the magnetization to steady state, 40 dummy scans were performed before data acquisition. For the mid-tibia, an 8-channel transmit-receive knee coil was used with FOV = 180×180 mm^2, sampling frequency bandwidth = ±83.3 kHz, 268 readout points for each half radial projection resulted in a reconstructed

matrix size of 512×512 and image resolution 0.35×0.35 mm^2. The Achilles tendon was imaged with a 4-channel receive-only ankle coil (Insight MRI, Boston, MA) with FOV = 120×120 mm^2, sampling frequency bandwidth = ±62.5 kHz, 205 readout samples for each half radial projection, reconstructed matrix size = 384×384 and pixel size = 0.31×0.31 mm^2. The body coil was used for RF transmission. To avoid confounding effects from the angle dependence of the collagen-bound water, the subjects were positioned horizontal and supine to ensure collagen fibers in the tendon aligned with the main magnetic field (33). Other acquisition parameters are listed in Table 1.

Image Reconstruction and Analysis

The acquired *k*-space data were remapped onto Cartesian grids using Greengard's regridding algorithm (34) before applying 2D IFFT. Prior to gridding, sampling density compensation weighting was performed. The weighting was calculated based on the gradient mapping (35) which measured the *k*-space trajectories. The final magnitude image was synthesized as the square-root of the sum-of-squares of the multi-coil images. The subtracted image was reconstructed as the magnitude image difference between the short- and long-TE images. The image reconstructions were implemented with MATLAB.

To quantitatively assess the performance of dual-echo UTE, dual-band UTE and IR-UTE, short-T_2 SNR and CNR were calculated. SNR was calculated as the ratio of the mean magnitude image intensity inside a user-defined region of interest to the standard deviation of the background signal. Typical regions of interest included more than 100 pixels. CNR was calculated as the difference between SNR of the tissue components of interest. For comparing sequences with different scan times, SNR was normalized by the square-root of total scan time to obtain *relative* SNR_{eff} with dual-echo UTE as the reference. We also calculated the ratio of short-T_2 SNR to surrounding long-T_2 SNR, a quantity measuring the level of short-T_2 retention and long-T_2 suppression.

Results

The off-resonance and T_2 profiles of the designed dual-band pulse are shown in Fig. 3. The dual-band pulse generates flip angles at water and fat bands of 100° and 110°, respectively (Fig. 3b). Since the bandwidth was designed large enough to compensate for field inhomogeneity and to cover the broad fat spectrum at 3T, its saturation effect on short T_2 species becomes substantial. The dual-band pulse is predicted to saturate 40% of cortical bone water (T_2 = 420 μs) and 60% of the tendon water protons (T_2 = 1 ms). Fig. 4 shows the off-resonance and T_2 profiles of the designed HS adiabatic pulse. As illustrated in Fig. 4b, a variation in RF amplitude by ±30% has negligible effect on the spectral profile of the pulse, demonstrating its insensitivity to B_1 inhomogeneity. However, Fig. 4c shows that short-T_2 signals are significantly attenuated. The residual longitudinal magnetizations of cortical bone water and tendon protons are on the order of 5% only immediately after the HS adiabatic pulse. Further, as T_2 shortens, the HS pulse gradually loses its insensitivity to B_1 variations (36).

The normalized theoretical SNR_{eff} of both cortical bone and tendon, as a function of TR for all three sequences, is shown in Figs. 5a and b, respectively. Imaging parameters used in the *in vivo* scans are indicated by markers in the figure. For each TR value the SNR_{eff} was calculated at the optimal flip angle of the excitation pulse. In IR-UTE, to obtain the SNR_{eff} dependence on TR, TI is selected as the time point for which the magnitude sum of fat and water signals achieves a minimum at a given TR. However, it is noted that the extent of soft-tissue suppression is TR dependent. For dual-band UTE, we used TR of 500 ms instead of optimal TR around 750 ms for tendon imaging, to trade off SNR efficiency gain and scan time.

Fig. 6 displays a representative comparison of left mid-tibia images from a 26-year-old healthy male volunteer using the three soft-tissue suppression methods with optimized image protocols. Fig. 6a shows the first echo image of dual-echo UTE in which the contrast between cortical bone and the surrounding tissue is poor. In dual-echo UTE (Fig. 6b), although the muscle signal is well suppressed, the bone marrow and subcutaneous fat signal are not removed by subtraction since T_2* of the lipid protons is on the order of the inter-echo time. Dual-band UTE yields considerably better short-T_2 contrast, but the soft-tissue suppression is not uniform across the FOV due to B_1 inhomogeneity, (Fig. 6c). When combining dual-band UTE with echo subtraction, better overall soft-tissue suppression is achieved (Fig. 6d). IR-UTE yields the highest contrast between short- and long-T_2 regions with homogeneous soft-tissue suppression (Fig. 6e). On the other hand, cortical bone SNR in IR-UTE is lowest.

Fig.7 shows images of the left Achilles tendon of a 38-year-old healthy male volunteer. Since the water density in tendon is substantially higher than that in bone, its signal intensity is comparable to the surrounding muscle tissue even without long-T_2 suppression. Otherwise, the relative benefits and trade-offs of the various suppression techniques are replicated for this short-T_2 tissue.

Table 2 quantitatively compares the performance of the three sequences in terms of the evaluation criteria used. Overall, dual-echo UTE yields the highest SNR_{eff} but the lowest contrast between short- and long-T_2 components. Relative to IR preparation dual-band saturation pulse preserves a greater fraction of short-T_2 signal. IR-UTE generates the highest contrast between short and long-T_2 tissues, albeit at the expense of short-T_2 SNR, which is lowest at this suppression scheme. This behavior is exacerbated when the short-T_2 protons have relatively long T_1, as in the case of tendons. Some discrepancies were observed between the simulations (Fig. 5) and experimental results (Table 2), particularly for the tendon images. Possible reasons are the presence of multiple T_2 components for tendon water protons, and deviations from the desired flip angle due to the tendon's off-center location.

Discussion

Soft-tissue suppression techniques employed in UTE imaging generate high short-T_2 contrast so as to reveal short-T_2 components ordinarily obscured by long-T_2 components. In this work, we attempted to compare the performance of three long-T_2 suppression UTE sequences in an unbiased manner via simulation and experiment. Results show that excellent short-T_2 contrast can be achieved when generated with these optimized sequences. Before drawing conclusions, we summarize the issues and discuss the applications for the soft-tissue suppression methods studied in this work.

Dual-echo UTE is the most commonly used soft-tissue suppression method. It is insensitive to both B_1 and B_0 inhomogeneities and is most SNR efficient as predicted theoretically and experimentally. This result is intuitive since no magnetization preparation is needed, which will always involve losses. Somewhat unexpected was the finding that background noise appears to be attenuated in multi-coil combined magnitude image subtraction, even though noise is amplified by $\sqrt{2}$ in a single-channel complex difference image. In fact, the noise level is amplified as expected by a factor of $\sqrt{2}$. However, since the mean of the background signal is substantially reduced after subtraction (all values before subtraction are strictly positive), the noise appears to be attenuated in the magnitude display (refer to Figs. 6(b), (d) and (f)). Additionally the subtraction operation may attenuate subtle streaking artifacts. The major problem with dual-echo UTE is the significant residual signal from species with T_2* comparable to the echo spacing, such as bone marrow and subcutaneous fat. Lipid protons

tend to have T_2* values as short as 10 ms resulting from destructive interference of their various chemically shifted components, and field inhomogeneity induced by susceptibility variations of the air-tissue and bone-soft tissue interfaces. Our data suggest that incorporation of dual-echo subtraction into magnetization preparation methods may be beneficial as a means to capitalize on the latter's complementary long-T_2 suppression properties.

With the optimized dual-band pulse, dual-band UTE achieves short-T_2 contrast superior to dual-echo UTE and higher SNR than IR-UTE. Since the UTE acquisition is played out immediately after the dual-band pulse, shorter scan time is possible than with IR-UTE which demands inclusion of an inversion delay. As well, the pulse design algorithm offers significant freedom to control the dual-band pulse, including flip angles, bandwidths and ripple values. In particular, frequency-band flip angles allow suppression of either long-T_2 component, which is not possible with a single-band saturation pulse. However, as all frequency-selective saturation pulses are, the dual-band pulse is sensitive to spatial variations in B_1 and B_0 fields, resulting in inhomogeneous soft-tissue suppression. A possible alternative is the use of 90° adiabatic pulses to address the B_1 sensitivity problem (37), but its saturation effect on short-T_2 species first needs to be investigated. To minimize sensitivity to B_0 inhomogeneity, larger bandwidths are required, particularly at high magnetic field, which in turn augment undesired saturation of the short-T_2 protons (15). To alleviate the pulse's sensitivity to B_1 and B_0 inhomogeneities and maximize soft-tissue suppression as demonstrated by our results, we recommend combining the dual-band UTE and echo subtraction method.

IR-UTE produces the highest short-T_2 contrast, achieved at the expense of SNR, which is lowest among the three long-T_2 suppression techniques. Soft-tissue suppression is uniform across the entire FOV due to the relative immunity of the adiabatic inversion pulse to B_1 inhomogeneity. In the present work the pulse was designed to achieve optimal soft-tissue suppression. Further, judicious choice of TR minimizes the TI difference between components differing in T_1. However, because of the time delay for long-T_2 inversion nulling, the scan time is relatively extensive compared to other sequences. Phase-sensitive IR (16) obviates the need for an inversion delay allowing for UTE acquisition immediately after the adiabatic inversion pulse. However, as shown in our simulations, saturation of the short-T_2 protons is significant, particularly in combination with long T_1 and increased pulse-bandwidth of the preparation pulse. Furthermore, two acquisitions with and without inversion preparation are required, which would double total scan time. Therefore, this method is not well suited in high-field applications since greater absolute field inhomogeneity and broader lipid spectrum necessitate larger pulse bandwidth. Also, because of the substantial saturation caused by the adiabatic pulse, the short-T_2 signal in IR-UTE mainly arises from longitudinal magnetization built up during the inversion time. This intuitively explains why half pulses with flip angles near 90 degrees are used in IR-UTE to maximize the short-T_2 signal. We further infer that IR-UTE may not be favorable to image short-T_2, long-T_1 species. Instead of a single adiabatic inversion pulse, two back-to-back pulses were used by Du et al. in DIR-UTE to suppress long-T_2 components with different T_1s (17). However, since the difference in inversion null times for water and fat is usually less than the duration of the long adiabatic pulse, TI for fat is suboptimal. Prolonging TR can partially rectify this problem, but at the expense of impractically long scan times. Another possible solution is to use dual-band adiabatic inversion pulse (38) to invert the long-T_2 components sequentially rather than simultaneously according to their TI difference. In (23), Du et al. conducted a comparison between the soft-tissue suppression schemes investigated in this work with 3D UTE imaging. Although the imaging parameters for each individual long-T_2 suppression method were not optimized and the comparison experiments were not carried out on the same anatomy due to long scan time of 3D UTE in (23), the

authors also concluded that IR-based UTE (IR-TUE or DIR-UTE) is a simple and efficient method that can relatively easily be implemented on clinical scanners. Based on our evaluation we conclude that IR-UTE is a low-SNR but high-CNR sequence with uniform soft-tissue suppression, which we favor for imaging short-T_2 species with relatively short T_1, such as cortical bone. The results of our performance evaluation and comparison among the various sequences are summarized in Table 3.

The short-T_2 SNR efficiency could be improved by acquiring multiple slices in an interleaved fashion. For the dual-echo UTE this mode of operation would increase SNR efficiency by a factor equal to the square-root of the number of slices acquired within a given TR period (just as in conventional multi-slice MRI). For dual-band UTE and IR-UTE, multiple slices can also be acquired within a TR period after each magnetization preparation pulse. However, this may result in somewhat impaired soft-tissue suppression across slices. Thus, there is a trade-off between SNR efficiency and extent of long-T_2 suppression when translating these soft-tissue suppression schemes into multislice mode.

The key motivation for soft-tissue suppression in UTE imaging is to enhance the visualization of short-T_2 tissues obscured by the overwhelming long-T_2 signal. More recently, soft-tissue-suppressed UTE imaging has been applied to directly quantify short-T_2 species, such as cortical bone water concentration (29), carotid plaque calcium (9,10) and myelin content (8). The motivation for incorporating long-T_2 suppression into UTE imaging is to avoid soft-tissue contamination because UTE imaging without suppression suffers from contamination of the signal from long-T_2 components or slice profile imperfections in 2D UTE. To decide on specific suppression schemes for short-T_2 imaging, the user will have to evaluate their performance and optimize the imaging parameters with SNR and CNR as the objective function. Also, as new soft-tissue suppression methods arise, it would seem appropriate to examine their performance against the methods evaluated in the present work to allow for unbiased comparison.

A limitation of this study is its focus on a comparison of short-T_2 SNR and CNR between short- and long-T_2 tissues for the three most widely used soft-tissue suppression methods in their 2D embodiments. Other methods, such as TELEX (12,13), DIR-UTE (17), were not evaluated and compared although they are variants of the methods investigated in this work. The sensitivity of these methods to pathologic changes of short-T_2 tissues remains to be examined to assess their clinical capabilities. Lastly, 3D implementations of the above sequences and their potential to visualize the microanatomy of collagen-rich short-T_2 tissues need to be investigated in future work.

Conclusion

In this work we have attempted to achieve an unbiased quantitative performance assessment of the three most commonly used soft-tissue suppression methods by optimizing imaging protocols by both simulation and measurements in phantoms and *in vivo*. IR-UTE provides the highest short-T_2 contrast and is well suited for imaging short-T_2 species with relatively short T_1. A combination of dual-band UTE with dual-echo UTE yields both good SNR and CNR and reduced sensitivity to B_1 inhomogeneity. The results provide a guide for the use of soft-tissue-suppressed UTE in research and in the clinic and the approach described may be useful for evaluating the performance of future soft-tissue suppression methods.

Acknowledgments

This work was supported by NIH grant RO1 AR50068.

References

1. Gatehouse PD, Bydder GM. Magnetic resonance imaging of short T2 components in tissue. Clin Radiol. 2003; 58(1):1–19. [PubMed: 12565203]
2. Pauly, JM.; Conolly, SM.; Nishimura, DG.; Macovski, A. Slice-selective excitation for very short T2 species.. Proceedings of SMRM, 8th Annual Meeting; Amsterdam. 1989; p. 28
3. Brittain, JH.; Shankaranarayanan, A.; Ramanan, V.; Shimakawa, A.; Cunningham, CH.; Hinks, S.; Francis, R.; Turner, R.; Johnson, JW.; Nayak, KS.; Tan, S.; Pauly, JM.; Bydder, GM. Ultra-short TE imaging with single digit (8us) TE.. Proceedings of the 12th Annual Meeting of ISMRM; Kyoto, Japan. 2004; p. 629
4. Techawiboonwong A, Song HK, Wehrli FW. In vivo MRI of submillisecond T(2) species with two-dimensional and three-dimensional radial sequences and applications to the measurement of cortical bone water. NMR Biomed. 2008; 21(1):59–70. [PubMed: 17506113]
5. Robson MD, Gatehouse PD, Bydder M, Bydder GM. Magnetic resonance: an introduction to ultrashort TE (UTE) imaging. J Comput Assist Tomogr. 2003; 27(6):825–846. [PubMed: 14600447]
6. Callaghan, PT. Principles of Nuclear Magnetic Resonance Microscopy. Oxford University Press; Oxford: 1995.
7. Bergin CJ, Pauly JM, Macovski A. Lung parenchyma: projection reconstruction MR imaging. Radiology. 1991; 179(3):777–781. [PubMed: 2027991]
8. Wilhelm, MJ.; Ong, HH.; Wehrli, SL.; Tsai, P-H.; Hackney, DB.; Wehrli, FW. Prospects for quantitative imaging of myelin with dual-echo short inversion time 3D UTE MRI.. Proceedings of ISMRM, 19th Annual Meeting; Montreal, Canada. 2011; p. 2460
9. Du J, Corbeil J, Znamirowski R, Angle N, Peterson M, Bydder GM, Kahn AM. Direct imaging and quantification of carotid plaque calcification. Magn Reson Med. 2010
10. Chan CF, Keenan NG, Nielles-Vallespin S, Gatehouse P, Sheppard MN, Boyle JJ, Pennell DJ, Firmin DN. Ultra-short echo time cardiovascular magnetic resonance of atherosclerotic carotid plaque. J Cardiovasc Magn R. 2010; 12:17.
11. Anumula S, Magland J, Wehrli SL, Zhang H, Ong H, Song HK, Wehrli FW. Measurement of phosphorus content in normal and osteomalacic rabbit bone by solid-state 3D radial imaging. Magn Reson Med. 2006; 56(5):946–952. [PubMed: 17041893]
12. Pauly, JM.; Conolly, SM.; Macovski, A. Suppression of long-T_2 components for short-T_2 imaging.. Proceedings of SMRM, 10th Annual Meeting; New York. 1992; p. 330
13. Sussman MS, Pauly JM, Wright GA. Design of practical T2-selective RF excitation (TELEX) pulses. Magn Reson Med. 1998; 40(6):890–899. [PubMed: 9840834]
14. Wu Y, Ackerman JL, Chesler DA, Graham L, Wang Y, Glimcher MJ. Density of organic matrix of native mineralized bone measured by water- and fat-suppressed proton projection MRI. Magn Reson Med. 2003; 50(1):59–68. [PubMed: 12815679]
15. Larson PE, Gurney PT, Nayak K, Gold GE, Pauly JM, Nishimura DG. Designing long-T2 suppression pulses for ultrashort echo time imaging. Magn Reson Med. 2006; 56(1):94–103. [PubMed: 16724304]
16. Larson PE, Conolly SM, Pauly JM, Nishimura DG. Using adiabatic inversion pulses for long-T2 suppression in ultrashort echo time (UTE) imaging. Magn Reson Med. 2007; 58(5):952–961. [PubMed: 17969119]
17. Du J, Takahashi AM, Bae WC, Chung CB, Bydder GM. Dual inversion recovery, ultrashort echo time (DIR UTE) imaging: creating high contrast for short-T(2) species. Magn Reson Med. 2010; 63(2):447–455. [PubMed: 20099332]
18. Du J, Takahashi AM, Bydder M, Chung CB, Bydder GM. Ultrashort TE imaging with off-resonance saturation contrast (UTE-OSC). Magn Reson Med. 2009; 62(2):527–531. [PubMed: 19449436]
19. Pauly J, Le Roux P, Nishimura D, Macovski A. Parameter relations for the Shinnar-Le Roux selective excitation pulse design algorithm. IEEE Trans Med Imaging. 1991; 10(1):53–65. [PubMed: 18222800]

20. Wu Y, Dai G, Ackerman JL, Hrovat MI, Glimcher MJ, Snyder BD, Nazarian A, Chesler DA. Water- and fat-suppressed proton projection MRI (WASPI) of rat femur bone. Magn Reson Med. 2007; 57(3):554–567. [PubMed: 17326184]
21. Wu Y, Hrovat MI, Ackerman JL, Reese TG, Cao H, Ecklund K, Glimcher MJ. Bone matrix imaged in vivo by water- and fat-suppressed proton projection MRI (WASPI) of animal and human subjects. J Magn Reson Imaging. 2010; 31(4):954–963. [PubMed: 20373441]
22. Rahmer J, Blume U, Bornert P. Selective 3D ultrashort TE imaging: comparison of “dual-echo” acquisition and magnetization preparation for improving short-T-2 contrast. Magn Reson Mater Phy. 2007; 20(2):83–92.
23. Du J, Bydder M, Takahashi AM, Carl M, Chung CB, Bydder GM. Short T2 contrast with three-dimensional ultrashort echo time imaging. Magn Reson Imaging. 2011; 29(4):470–482. [PubMed: 21440400]
24. Techawiboonwong A, Song HK, Leonard MB, Wehrli FW. Cortical bone water: in vivo quantification with ultrashort echo-time MR imaging. Radiology. 2008; 248(3):824–833. [PubMed: 18632530]
25. Rad HS, Lam SC, Magland JF, Ong H, Li C, Song HK, Love J, Wehrli FW. Quantifying cortical bone water in vivo by three-dimensional ultra-short echo-time MRI. NMR Biomed. 2011
26. Robson MD, Benjamin M, Gishen P, Bydder GM. Magnetic resonance imaging of the Achilles tendon using ultrashort TE (UTE) pulse sequences. Clin Radiol. 2004; 59(8):727–735. [PubMed: 15262548]
27. Du J, Pak BC, Znamirowski R, Statum S, Takahashi A, Chung CB, Bydder GM. Magic angle effect in magnetic resonance imaging of the Achilles tendon and enthesis. Magn Reson Imaging. 2009; 27(4):557–564. [PubMed: 19022600]
28. Jaynes ET. Matrix Treatment of Nuclear Induction. Phys Rev. 1955; 98(4):1099–1105.
29. Du J, Carl M, Bydder M, Takahashi A, Chung CB, Bydder GM. Qualitative and quantitative ultrashort echo time (UTE) imaging of cortical bone. J Magn Reson. 2010; 207(2):304–311. [PubMed: 20980179]
30. Smith, MJ.; Li, C.; Bhagat, YA.; Lam, S.; Love, JH.; Wehrli, FW. Implications of soft-tissue suppression on cortical bone water signal in ultrashort echo-time imaging.. Proceedings of ISMRM, 19th Annual Meeting; Montreal, Canada. 2011; p. 1131
31. Conolly S, Nishimura D, Macovski A, Glover G. Variable-Rate Selective Excitation. J Magn Reson. 1988; 78(3):440–458.
32. Pauly, JM. Design of large-flip-angle half pulse.. Proceedings of ISMRM, 14th Annual Meeting; Seattle. 2006; p. 2997
33. Bydder M, Rahal A, Fullerton GD, Bydder GM. The magic angle effect: a source of artifact, determinant of image contrast, and technique for imaging. J Magn Reson Imaging. 2007; 25(2): 290–300. [PubMed: 17260400]
34. Greengard L, Lee JY. Accelerating the nonuniform fast Fourier transform. Siam Rev. 2004; 46(3): 443–454.
35. Magland, JF.; Rad, HS.; Wehrli, FW. Correcting for gradient imperfections in ultra-shoft echo time imaging.. Proceedings of ISMRM, 18th Annual Meeting; Stockholm, Sweden. 2010; p. 3102
36. Norris DG, Ludemann H, Leibfritz D. An Analysis of the Effects of Short T2 Values on the Hyperbolic-Secant Pulse. J Magn Reson. 1991; 92(1):94–101.
37. Johnson AJ, Garwood M, Ugurbil K. Slice Selection with Gradient-Modulated Adiabatic Excitation Despite the Presence of Large B1-Inhomogeneities. J Magn Reson. 1989; 81(3):653–660.
38. Goelman G. Two methods for peak RF power minimization of multiple inversion-band pulses. Magn Reson Med. 1997; 37(5):658–665. [PubMed: 9126939]

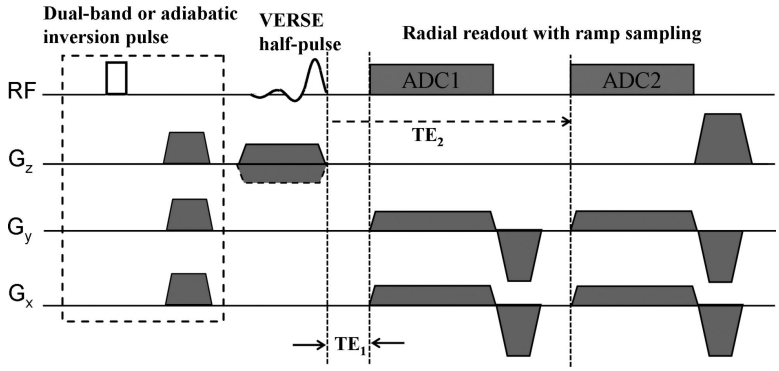

Figure 1.

2D UTE pulse sequence with soft-tissue suppression. In dual-echo UTE two identical half-radial projections differing in echo time are acquired after each half-pulse excitation. The dashed box indicates the magnetization-preparation portion of long-T_2 suppression, in which a dual-band pulse (dual-band UTE) or adiabatic inversion pulse (IR-UTE) followed by a spoiler gradient is applied before standard UTE acquisition. For IR-UTE, an inversion time (not shown here) is inserted to null the longitudinal magnetization before UTE acquisition.

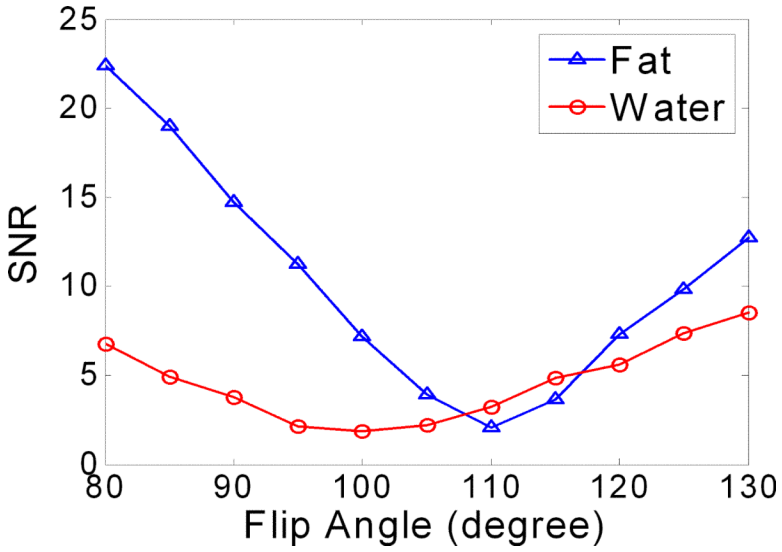

Figure 2.
SNR for doped water and vegetable oil vs. flip angle of the conventional dual-band pulse. The optimum flip angles are different for water (100 degrees) and fat (110 degrees), reflecting their different relaxation times and spectral bandwidths.

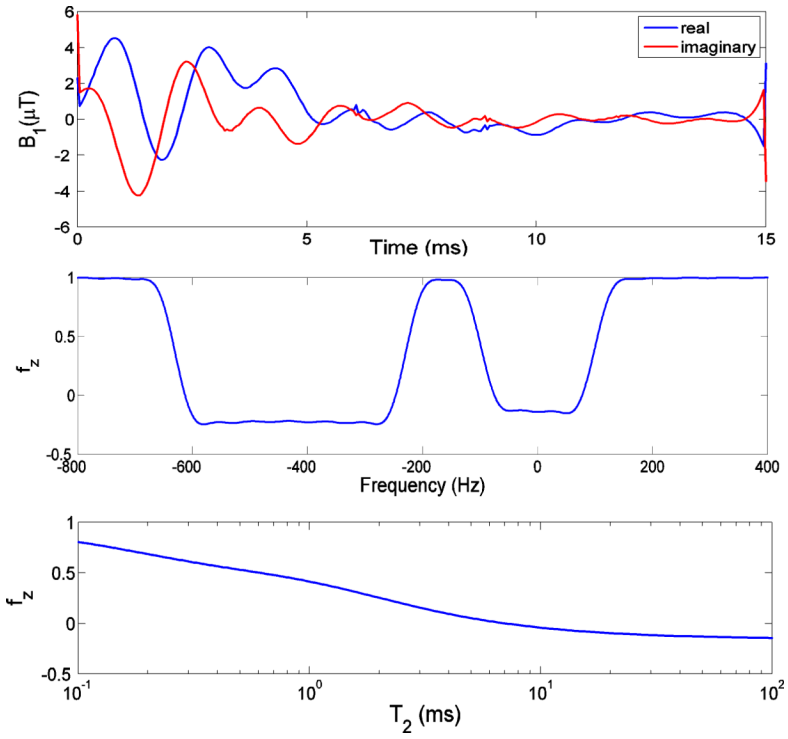

Figure 3.

Bloch equation simulations of (a) 15 ms dual-band pulse. (b) Off-resonance profile for T_2 = 100 ms, T_1 = 1 s. The dual-band pulse had a suppression bandwidth of 120 Hz with flip angle of 100° on resonance with water and bandwidth of 320 Hz with flip angle of 110° at the fat resonance centered at -430 Hz. (c) On-resonance T_2 profile. Due to the increased suppression bandwidth at 3T, 40% of cortical bone water (T_2 = 420 μs) and 60% of the tendon signal (T_2 = 1ms) are saturated.

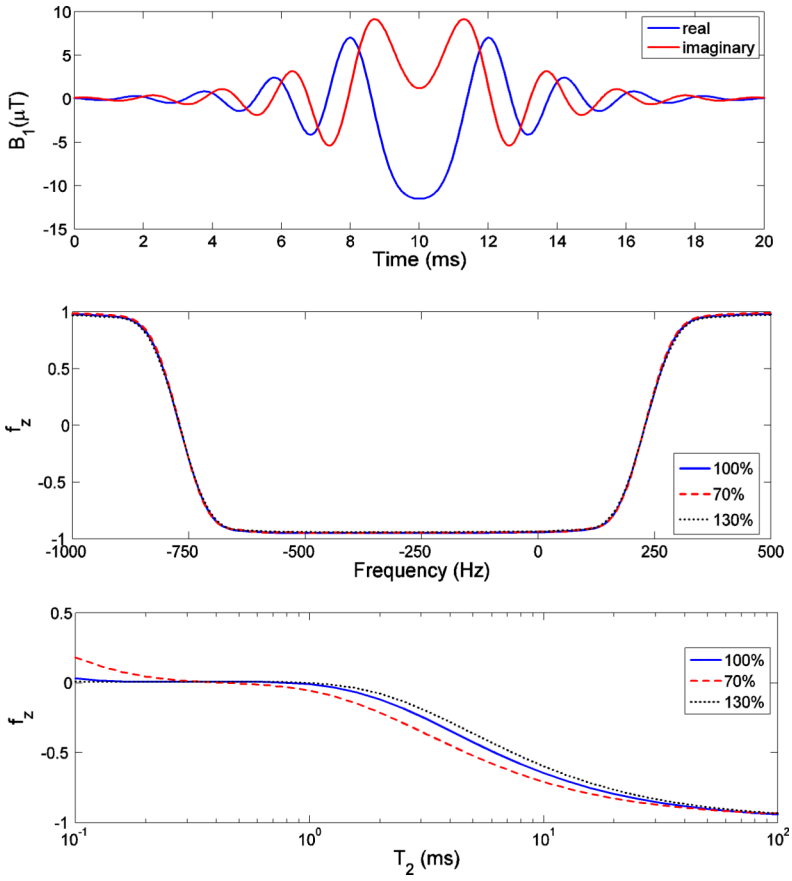

Figure 4.

Bloch equation simulations of (a) 20 ms HS pulse with bandwidth of 1 kHz. (b) Off-resonance profile for T_2 = 100 ms, T_1 = 1 s. The HS pulse is shifted 270 Hz towards the lipid peak to cover both fat and water peaks. The solid line was calculated at the desired B_1 amplitude. The dashed and dotted lines correspond to 70% and 130% of the desired amplitude, respectively. For B_1 variations of up to 30% the frequency profile of the HS pulse changes negligibly. (c) On-resonance T_2 profile: less than 5% longitudinal magnetization remains for protons with $T_2 \leq 1$ ms upon application of the HS adiabatic pulse.

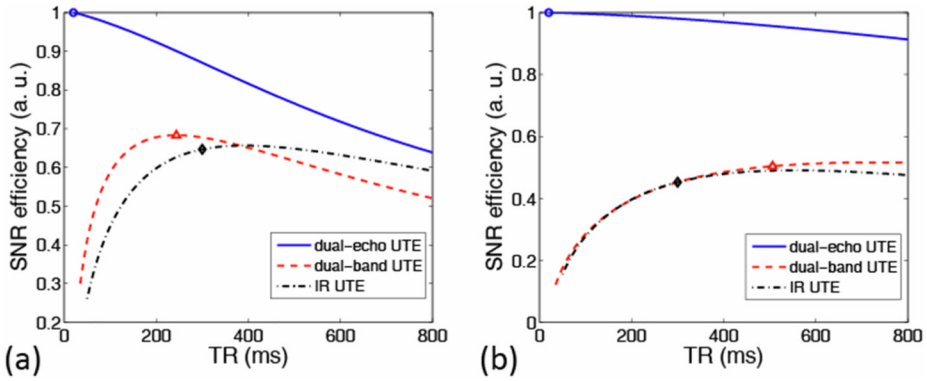

Figure 5.

Normalized theoretical SNR efficiencies for (a) cortical bone and (b) tendon as a function of *TR* for the three sequences. Short-T_2 SNR efficiency is highest for dual-echo UTE (solid line) but generally lower for dual-band UTE (dashed line) and IR-UTE (dashed-dotted line) due to perturbation of the spin system by the magnetization preparation pulses. The imaging parameters used in the *in vivo* scans are indicated by markers: circle: dual-echo UTE; triangle: dual-band UTE; diamond: IR-UTE.

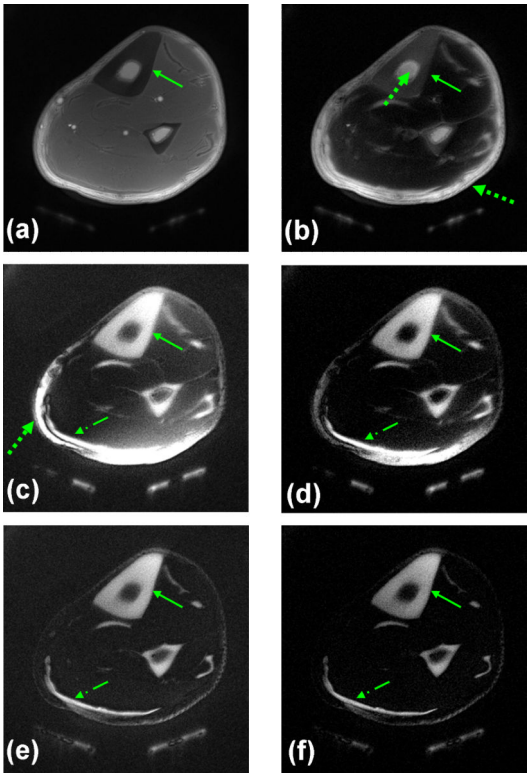

Figure 6.
Axial mid-tibia images of a healthy volunteer: a, b) dual-echo UTE; c, d) dual-band UTE; e, f) IR-UTE. Left column (a, c, e): first-echo images; right column (b, d, f): difference images (first minus second-echo). Cortical bone (thin arrow) is obscured by the surrounding intense soft-tissue signal, but highlighted in the long-T_2 suppressed images. The tendon signal also appears enhanced (dotted-dashed arrow). There is significant residual fat signal in dual-echo UTE (dashed arrow in (b)). Dual-band UTE has high short-T_2 SNR but its soft-tissue suppression is inhomogeneous (dashed arrow in (c)). Cortical bone contrast is highlighted and uniform in IR-UTE (e, f). For better comparison, (c, d, e, f) are on the same window/level. Signal extraneous to the boundaries of the calf is from polymeric structures of the coil.

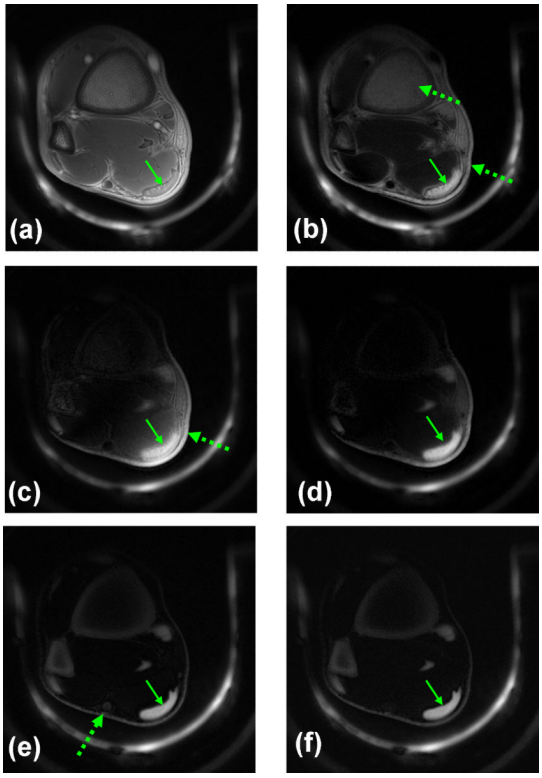

Figure 7.
Axial lower-extremity images of a healthy volunteer: a, b) dual-echo UTE, c, d) dual-band UTE: e, f) IR-UTE. Left column (a, c, e): first-echo images; right column (b, d, f): difference images (first minus second-echo). Contrast between Achilles tendon (thin arrow) and muscle is poor without soft-tissue suppression. Considerable residual fat signal appears in dual-echo UTE (dashed arrow in b)). Soft-tissue suppression is inhomogeneous (dashed arrow in c)) but it is improved when combined with dual-echo UTE (d). IR-UTE creates the highest and most homogeneous tendon contrast. Residual blood signal is visible (dotted arrow in (e)) due to its long T_1. The image window levels for echo row images are individually adjusted for better visualization since the image SNRs are substantially different from each other (see Table 2). Signal extraneous to the anatomy is from proton-containing structures of the ankle coil.

Table 1

Imaging Parameter Sets for Dual-echo UTE, Dual-band UTE and IR-UTE Used in the *in vivo* Experiments

	Cortical Bone	Tendon
dual-echo UTE	TR = 20 ms, FA = 25°	TR = 20 ms, FA = 15°
dual-band UTE	TR = 240 ms, FA = 75°	TR = 500 ms, FA = 76°
IR-UTE	TR = 300 ms, TI = 100 ms, FA = 87°	TR = 300 ms, TI = 100 ms, FA = 89°

Table 2

Quantitative Comparison of Three Long-T_2 Suppression Sequences, Including Absolute SNR of Cortical Bone (SNR_{bone}) and Achilles Tendon (SNR_{tendon}), CNR Between Cortical Bone and Muscle (CNR^{muscle}_{bone}), Cortical Bone and Marrow (CNR^{marrow}_{bone}), Achilles Tendon and Muscle (CNR^{muscle}_{tendon}), Relative SNR Efficiencies of Cortical Bone (SNR^{eff}_{bone}) and Achilles Tendon (SNR^{eff}_{tendon}), SNR Ratios of Cortical Bone to Muscle ($\frac{SNR_{bone}}{SNR_{muscle}}$), Cortical Bone to Marrow ($\frac{SNR_{bone}}{SNR_{marrow}}$), and Achilles Tendon to Muscle ($\frac{SNR_{tendon}}{SNR_{muscle}}$), Expressed as Means ± Standard Deviation from Five Subjects.

	Cortical Bone						Tendon			
	SNR_{bone}	CNR^{muscle}_{bone}	CNR^{marrow}_{bone}	SNR^{eff}_{bone}	$\frac{SNR_{bone}}{SNR_{muscle}}$	$\frac{SNR_{bone}}{SNR_{marrow}}$	SNR_{tendon}	CNR^{muscle}_{tendon}	SNR^{eff}_{tendon}	$\frac{SNR_{tendon}}{SNR_{muscle}}$
dual-echo UTE	25.6±2.7	15.6±1.1	-42.4±2.4	1.00	2.56	0.38	140.5±17.4	126.5±9.1	1.00	10.0
dual-band UTE	32.1±7.3	20.7±6.6	16.3±7.0	0.72	2.84	2.03	172.2±34.6	160.0±29.0	0.49	14.1
IR-UTE	26.1±5.0	20.2±4.5	17.1±3.0	0.53	4.42	2.90	86.5±7.2	81.4±7.2	0.32	17.0

Table 3

Relative Performance of Three Soft-Tissue Suppression Sequences: -/=/+ Scale Indicating Poorest to Best

Performance criterion	dual-echo UTE	dual-band UTE	IR-UTE
Short-T_2 SNR	+	=	-
Long-T_2 suppression	-	=	+
Robustness to B_0 inhomogeneity	+	=	=
Robustness to B_1 inhomogeneity	+	-	+
Scan time	+	=	-